Strategies to Improve Electrical and Ionic Conductivities of Metal–Organic Frameworks

Monica A. Gordillo and Sourav Saha*

Department of Chemistry, Clemson University, 211 S. Palmetto Blvd, Clemson, SC 29634

Email: souravs@clemson.edu

Abstract. Owing to their highly ordered crystalline structures and ease of introducing different electroactive meta ions and ligands, metal–organic frameworks (MOFs) have emerged as promising electrical and ion conducting materials. In this minireview, we highlighted recent advances in guest-induced electronic and ionic conductivity of MOFs, which are otherwise insulators or poor conductors. Examples of conductivity enhancement upon guest-induced framework oxidation or reduction, π-donor/acceptor stack formation, crosslinking of coordinatively unsaturated nodes, and binding of mobile Li^+ and Mg^{2+} with the MOFs are discussed.

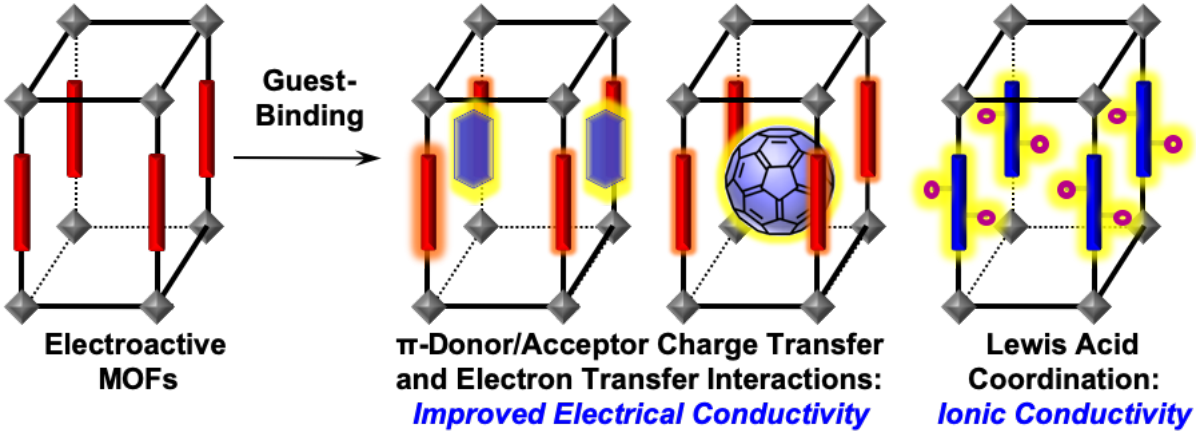

1. Introduction

Composed of metal clusters nodes and organic linkers, metal organic frameworks (MOFs) have emerged as versatile platforms with unparalleled chemical and structural tunability, synthetic facility, permanent porosity, and size-selective guest encapsulation capability.[1–3] These characteristics make them potential candidates for a range of diverse applications such as gas storage,[4] drug delivery,[5] catalysis[6,7] and sensing,[7,8] which are now well documented. In recent years, the introduction of redox- and photoactive components have yielded stimuli-responsive electronic and photonic MOFs and opened the door for myriad molecular electronics applications.[9,10] Electrical and ionic conductivities are among the most coveted and challenging properties of MOFs, which are vital for their potential applications in future molecular electronics and photovoltaic devices.[11] However, most porous MOFs developed to date have poor intrinsic conductivity due to inadequate charge carrier concentration and mobility.[10,12–14] Furnishing MOFs with electroactive metal ions and ligands addresses the first criterion by enriching them with mobile charge carriers, but their presence alone does not necessarily make MOFs conducting until the charge carriers can move freely through well-defined pathways (either through-bond or through-space), which is a challenging proposition in porous MOFs.[9–14] Although a number of 2D graphitic MOFs[15–20] have been developed recently that display remarkably high intrinsic conductivity—a feature that is vital for their applications as viable electronic materials[21–25]—3D porous frameworks[26–29] continue to lag far behind. One way to improve the conductivity of 3D porous MOFs is to introduce complementary guest molecules[30] that would not only endow MOFs with mobile charge carriers, but also create either through-bond or through-space long range charge movement pathways. In this review, we will focus our discussion on some representative examples of guest-induced conductivity manipulation strategy, which takes advantage of MOF's porosity to create a non-native property.

2. Guest-Induced Electrical Conductivity

2.1. I_2-Induced Anisotropic Electrical Conductivity of $\{Zn_3(_{DL}\text{-lac})_2(pybz)_2]\bullet 2.5DMF\}_n$ MOF

In one of the earliest reports of electrically conducting frameworks, Zeng et al.[31] synthesized a new MOF consisting of two different organic linkers, which served different roles within the structures: The lactate anion ($_{DL}$-lac) acted as rigid metal-organic pillars while 4-pyridylbenzoate (pybz) as aromatic walls forming a non-conductive, non-interpenetrated double-walled MOF $\{Zn_3(_{DL}\text{-lac})_2(pybz)_2]\bullet 2.5DMF\}_n$ (**1**) with inner channel dimensions of 11.2 × 10.2 Å in the as-synthesized material and 10.5 × 10.5 Å in the evacuated form (Figure 1). After treating the evacuated material **1′** with I_2/hexane solution, the mass of the material doubled, which corresponded to loading of three I_2 molecules per formula unit of **1′**. The calculated density

of **1′⊃3I₂** (2.48 g/cm^3) suggested a highly ordered arrangement of guest I_2 molecules, which were aligned in four close parallel chains within the channels of **1′**. The crystallinity and surface area of the iodine-treated MOF diminished noticeably. The **1′⊃3I₂** crystals showed anisotropic electrical conductivities: 3.42×10^{-3} S/cm along the channels and 1.64×10^{-4} S/cm perpendicular to the channels, which were notably greater than the reported electrical conductivity of I_2. The anisotropic factor of 21 was attributed to a highly ordered arrangement of the encapsulated I_2 molecules along the channels, which were responsible for the charge transfer process causing the improved electrical conductivity. Although the pristine MOF was not particularly conducting, it served as a templating host for organizing the guest I_2 molecules and engaged them in donor-acceptor interactions with the aromatic walls, enabling anisotropic electrical conductivity.

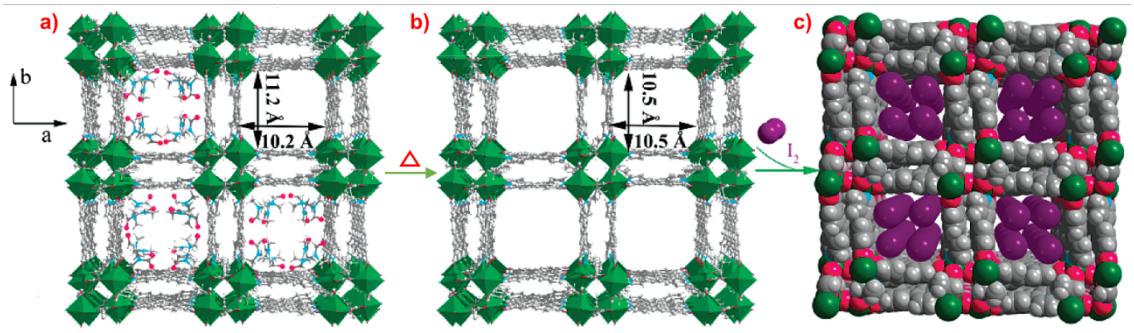

Figure 1. a) As synthesized $\{Zn_3(_{DL}\text{-lac})_2(pybz)_2]\bullet2.5DMF\}_n$ (**1**) with DMF molecules inside the channels b) **1'** showing the symmetric channels after desolvation and c) **1'** filled with ordered I_2 molecules along the channels. Adapted from reference 31.

2.2. I_2-Induced Electrical Conductivity of Cu[Ni(pdt)$_2$] MOF

In the same year, Allendorf and Long[32] reported a new 3D microporous Cu[Ni(pdt)$_2$] (pdt = pyrazine-2,3 dithiolate) MOF containing electron rich Ni(pdt)$_2$ ligands (Figure 2a), which imparted its redox property to the resulting MOF and enabled conductivity enhancement upon I_2-induced framework oxidation. Unlike the previous example where the guest I_2 molecules did not trigger any formal redox process, I_2 partially oxidized this MOF rendering it electrically more conductive. Interestingly, the iodine-treated MOF remained crystalline, as evident from its PXRD pattern. The room temperature conductivity of the as-synthesized Cu[Ni(pdt)$_2$] was 1×10^{-8} S/cm (Figure 2b), which was lower than a previously reported isostructural Cu[Cu(pdt)$_2$] MOF due to a lower charge density and a higher redox potential of the $[Ni(pdt)_2]^{2-/1-}$ couple. However, upon exposing a Cu[Ni(pdt)$_2$] film to a stream of I_2 vapor at 50 °C the *in-situ* measured conductivity increased 10^4 fold to 1×10^{-4} S/cm (Figure 2b), which was also accompanied by a 2.7 times lower activation energy. The conductivity enhancement upon doping Cu[Ni(pdt)$_2$] with an

oxidizing molecule, I_2, implied that the MOF was a p-type semiconductor. Furthermore, the authors claimed that charge conduction took place through the framework, not through the guest I_2 molecules, which was evident from the fact that very small amount of I_2 was found within the MOF and the MOF remained microporous.

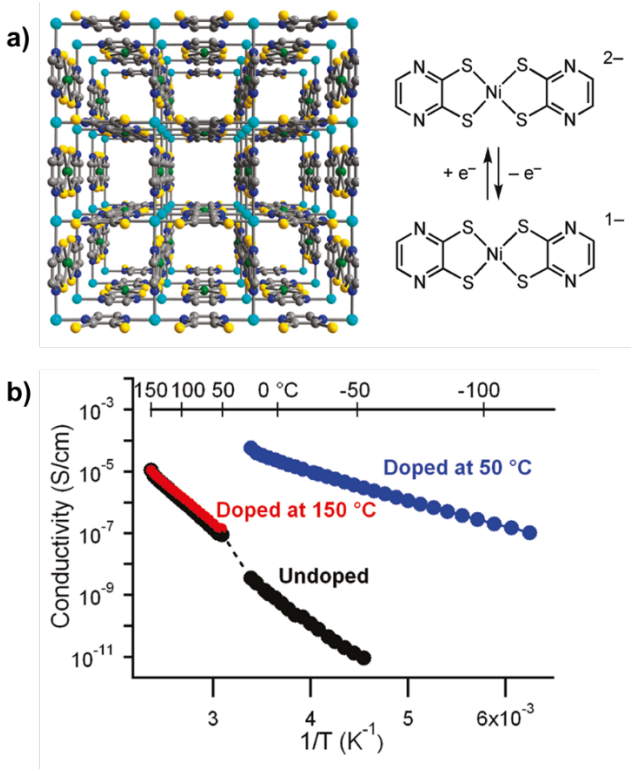

Figure 2. a) $Cu[Ni(pdt)_2]$ structure and redox behavior of the Ni(II) bis-dithiolate complexes within the framework and b) Temperature dependent conductivity of the undoped and doped MOF films. Adapted from reference 32.

2.3. I_2-Induced Electrical Conductivity of $Co_3(NDC)_3$ MOF

Han et al.[33] also demonstrated I_2-induced conductivity enhancement of $Co_3(NDC)_3$ MOF (NDC = 2,6-naphthalenedicarboxylate) thin-films deposited on amine-functionalized glass substrates by doctor-blade (DB) and layer-by-layer (LbL) techniques (Figure 3). While the pristine MOF films behaved as insulators due to poor charge carrier density, upon loading of 0.35 I_2 molecules per unit cell of $Co_3(NDC)_3$ MOF, the electrical conductivity of both films increased noticeably. The layer-by-layer grown MOF films displayed slightly higher conductivity (1.88×10^{-6} S/cm) than the doctor-blade films (10^{-7} S/cm) possibly because of the presence of fewer grain boundaries in the former. The conductivity exhibited by the doped films was attributed to I_2-mediated oxidation of NDC ligands, which created charge carrier holes within the

framework. The oxidation of the electron rich ligands by I_2 in the doped films was confirmed by the emergence of characteristic XPS signals of I_3^- and a broad donor/acceptor charge-transfer band indicating NDC/I_2 interaction by UV-Vis spectroscopy. Furthermore, the authors demonstrated that the I_2-doped $Co_3(NDC)_3$ films grown on conductive ITO substrates could act as light-harvesting materials.

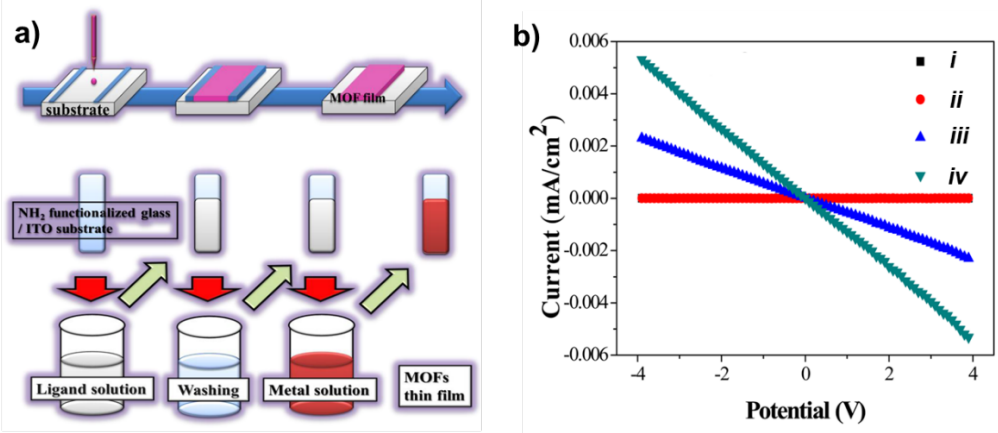

Figure 3. a) $Co_3(NDC)_3$ MOF's thin film fabrication using Doctor-Blade (top) and Layer-by-Layer (bottom) methods. b) I-V curves of $Co_3(NDC)_3$ MOF films on glass substrate (*i*) D-B film undoped, (*ii*) LbL film undoped, (*iii*) D-B film I_2 doped and (*iv*) LBL film I_2 doped. Adapted from reference 33.

2.4. TCNQ-Induced Electrical Conductivity of HKUST-1 MOF

Another strategy to enhance the electrical conductivity of intrinsically insulating MOFs involved creating through-bond charge transport pathways by introducing coordinating guests that could crosslink the coordinatively unsaturated nodes. Allendorf et al.[34] demonstrated this strategy by doping films of activated $Cu_3(BTC)_2$ (BTC: benzene-1,3,5,-tricarboxylic acid), also known as HKUST-1, with conjugated TCNQ (7,7,8,8-tetracyanoquinododimethane) guest molecules. Upon TCNQ doping, the PXRD signals of HKUST-1 became broader and lower in intensity, indicating diminished crystallinity. The electrical conductivity of TCNQ doped HKUST-1 surged to 7×10^{-2} S/cm from mere 1×10^{-8} S/cm recorded for the undoped material. This enhancement was attributed to the replacement of axially coordinated H_2O molecules from the $Cu_2(COO)_4$ paddlewheel nodes with TCNQ guest molecules, which crosslinked the nodes, enabling electronic coupling between the Cu centers of different nodes (Figure 4). The charge transfer interactions between the cross-linked TCNQ molecules and $Cu_3(BTC)_2$ MOF were confirmed by two new broad absorption bands in the 700-850 nm region. Additional experiments revealed that confinement of the TCNQ molecules in the MOF pores was mandatory for the formation of charge transfer complexes between Cu and TCNQ. DFT modeling and Raman spectroscopy also confirmed the binding of

the TCNQ molecules to the Cu(II) centers in the MOF. Furthermore, experiments with geometrically similar, but electronically different guest molecules demonstrated the importance of host-guest interactions and through-bond charge transport on improved conductivity: For example, the introduction of saturated version of TCNQ, H_4-TCNQ, which lacked conjugation, led to low conductivities similar to the undoped MOF, as it failed to support resonance delocalization. The introduction of fluorinated version F_4-TCNQ led to a higher electrical conductivity compared to the pristine evacuated MOF, but it was still much lower than the TCNQ-doped $Cu_3(BTC)_2$ MOF, presumably because of a higher electron affinity of the F_4-TCNQ, which impeded the electron mobility through the framework.

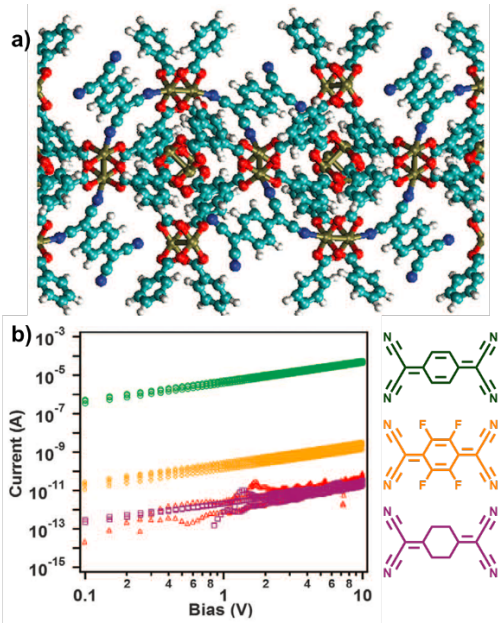

Figure 4. a) $Cu_3(BTC)_2$ MOF furnished with cross-linking TCNQ guest molecules that permitted through-bond charge transfer. b) The I-V profiles of undoped and doped $Cu_3(BTC)_2$ showing guest-specific electrical conductivity of the MOF. Adapted from reference 34.

2.5. Methyl Viologen (MV^{2+})-Induced Electrical Conductivity of BMOF

We have developed a new strategy to enhance the electrical conductivity of MOFs composed of redox-active ligands by introducing complementary guest π-systems.[35] Intercalation of complementary guest molecules between the pre-organized ligands leading to the formation of extended π-donor/acceptor stacks facilitated through-space electron delocalization within the framework and led to improved conductivity. To demonstrate this widely adoptable strategy, we constructed a new blue-colored electroactive pillared-paddlewheel MOF [Zn_2(TCPB)(BPDPNDI)], named BMOF, composed of electron rich *N,N'*-bis(4-

pyridyl)-2,6-dipyrrolidyl naphthalenediimide (BPDPNDI) pillars and 1,2,4,5-tetrakis-(4-carboxyphenyl)benzene (TCPB) struts (Figure 5). Stable BMOF films were grown solvothermally on ZnO-coated glass substrates equipped with four interdigitated Au-electrodes, and the effects of various guests π systems, such as electron deficient dinitrotoluene (DNT), difluoro-dinitro-benzene (DFDNB), π acidic methyl viologen (MV^{2+}) and C_{60}, as well as electron rich N-methyl-phenothiazine (NMPTZ) and TTF on the electrical conductivity were investigated. The four probe electrical measurement revealed a poor conductivity of pristine BMOF film (6×10^{-7} S/cm), which underwent a 40-fold enhancement to 2.3×10^{-5} S/cm upon infiltration of strongly π acidic MV^{2+} guest and much smaller (2–3 fold) improvement after infiltration of weaker π acidic guests DNT and DFDNB. The guest-dependent conductivity enhancement was attributed to improved charge transport through the guest-mediated π-donor/acceptor stacks, among which, the BPDPNDI/MV^{2+} stacks were the most effective. In contrast, electron rich guests such as TTF and NMPTZ did not improve the conductivity of BMOF films due to electronic mismatch. Likewise, large C_{60} molecules also did not affect the conductivity of BMOF, as they were size excluded. Together, these results demonstrated that both size and electronic complementarity between the MOF and guest molecules are needed to create effective π-donor/acceptor stacks that can promote through-space charge mobilization and thereby improve the MOF conductivity.

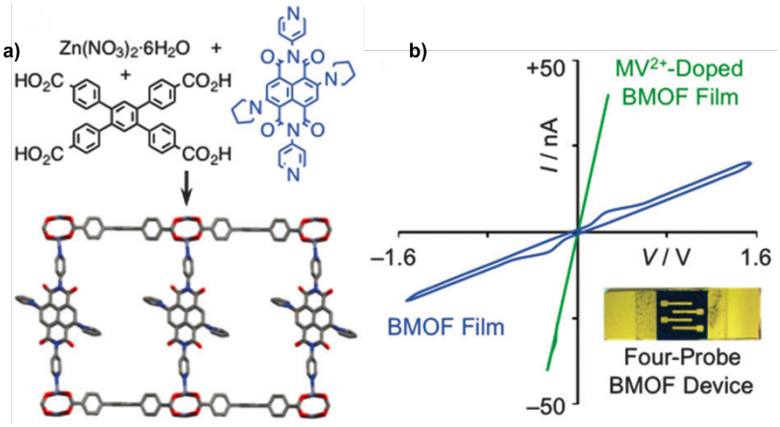

Figure 5. a) Synthesis and crystal structure of BMOF and b) I-V profiles of undoped (blue line) and MV^{2+}-doped (green line) BMOF. Adapted from reference 35.

2.6. TTF-Induced Electronic Bandgap Reduction of DSNDI-based MOF-74

We demonstrated the versatility of this strategy by employing a honeycomb-shaped MOF-74 (Figure 6) analog based on an electron deficient naphthalenediimide ligand functionalized with two salicylic acid groups (DSNDI).[36] In this MOF-74 analog, the DSNDI ligands were stacked along the c-axis ~6.5–7 Å

apart. This interligand distance was too large for effective π–π-interaction among themselves, but suitable for the intercalation of complementary planar π-systems, which could create extended π-donor/acceptor stacks along the c-axis and facilitate charge delocalization. As a result, the intercalation of electron rich planar tetrathiafulvalene (TTF) between the DSNDI ligands lowered the optical band gap of the parent material from 2.5 to 1.5 eV. Evidence of electronic communication between the guest-host couple also came from EPR spectroscopy. While the pristine neutral MOF was EPR silent, it became EPR active upon TTF infiltration, indicating paramagnetic $TTF^{\bullet+}$ radical cation and $DSNDI^{\bullet-}$ radical anion formation via partial charge transfer from TTF to DSNDI. The UV-Vis absorption and diffuse reflectance spectra also revealed TTF/NDI charge-transfer interaction, confirming that TTF molecules were indeed intercalated between the NDI ligands forming π-donor/acceptor stacks, which facilitated charge delocalization. DFT calculations further revealed orbital interaction between the stacked NDI ligands and TTF guests, which comprised the valence and conduction bands of the TTF-doped MOF. As a result, the electronic band gap of TTF-doped MOF-74 (1.5 eV) was 1 eV narrower than that of pristine MOf-74 (2.5 eV), suggesting that former should have higher electrical conductivity.

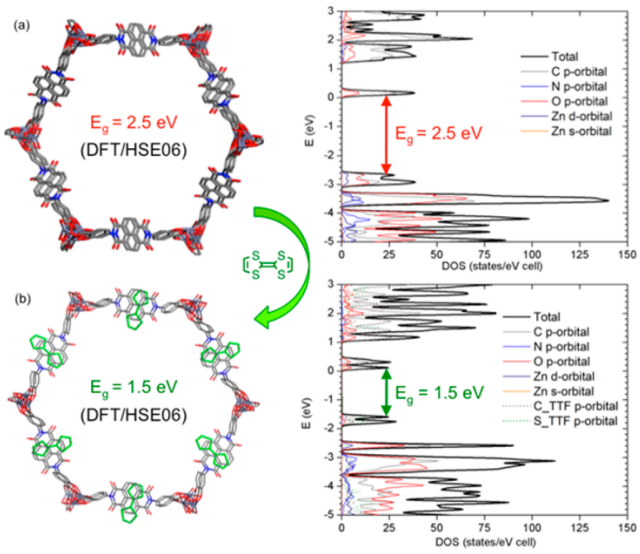

Figure 6. DFT simulated structures (left) and corresponding band structures (right) of DSNDI-based MOF 74 a) in the absence and b) in the presence of TTF guests intercalated between the electron deficient DSNDI ligands. Adapted from reference 36.

2.7. C_{60}-Induced Electrical Conductivity of NU-901 MOF

Farha et al.[37] also demonstrated the same concept by introducing electron deficient C_{60} guests into diamond shaped pores of NU-901 (Figure 7) composed of electron rich 1,3,6,8-tetrakis(*p*-benzoate)pyrene ($TBAPy^{4-}$

) ligands. The presence of C_{60} guests inside NU-901 pores (0.6 C_{60} molecules per node) was confirmed by Raman spectroscopy, and π-donor/acceptor charge transfer interaction was observed by UV-Vis and photoluminescence spectra. The electrical conductivity of undoped and C_{60}-doped NU-901 was determined from two-point *I-V* measurements performed on pressed pellets, which revealed 10^{11} times improvement from 10^{-14} S/cm measured for pristine NU-901 to ~ 10^{-3} S/cm after C_{60} incorporation. Such remarkable conductivity enhancement was attributed to pyrene/C_{60} π-donor/acceptor charge transfer interactions, which was also supported by DFT band calculations showing the electronic bandgap reduction after C_{60} installation. The porosity and internal surface area of NU-901 dropped 27% after C_{60} encapsulation.

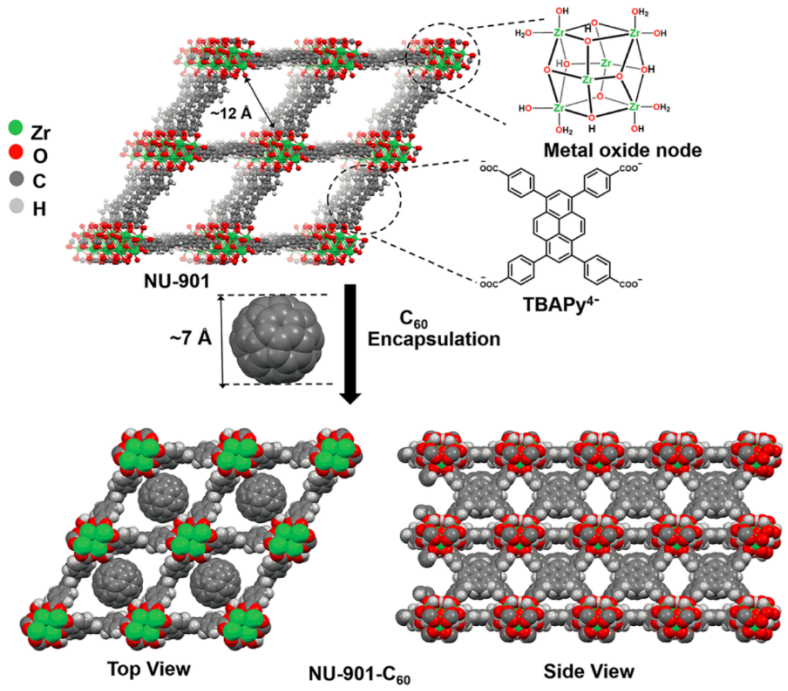

Figure 7. NU-901 MOF structure showing the individual components as well as DFT optimized top and side views assuming 1:1 occupancy of the C_{60} molecules inside the diamond shape pores. Adapted from reference 37.

2.8. Nickel(IV)bis(dicarbollide)-Induced Electrical Conductivity of NU-1000 MOF

The porosity of MOFs is usually diminished upon inclusion of guest molecules inside the pores. While this may not be an issue when the goal is just to enhance the electrical conductivity of porous frameworks, it could be detrimental for their electrocatalysis applications, which requires size-selective inclusion of substrate molecules inside electroactive MOF cavities containing the catalytic sites. To address this issue, Farha et al.[38] employed NU-1000 MOF made of pyrene ligands and Zr_6 nodes (Figure 8), which possessed

two different sized pores—one-dimensional hexagonal mesoporous channels and triangular microporous channels—where different guests can reside selectively based on their sizes. First, Ni(IV) bis(dicarbollide) (NiCB) guests were introduced into NU-1000 with a loading of 0.74±0.07 NiCB molecules per node, as measured by ICP-OES. Single-crystal X-ray diffraction analysis confirmed that NiCB molecules occupied the triangular microporous channels between three pyrene molecules. Although the influx of NiCB into NU-1000 diminished its BET surface from 2215 m^2/g to 1260 m^2/g, the resulting material still exhibited mesoporosity thanks to the empty hexagonal channels. Electrochemical impedance spectroscopy (EIS) revealed the electrical conductivity of spin-coated thin-film of NiCB-doped MOF (NiCB@NU-1000) to be 2.7×10^{-7} S/cm (the conductivity of the insulating parent NU-1000 was not measurable), which was attributed to donor/acceptor charge transfer between the pyrene linkers and NiCB guests within the framework. Even though the conductivity of NiCB@NU-1000 was still rather low, the unoccupied hexagonal channels left open the possibility of incorporation of other species, which could lead to other applications such as electrocatalysis.

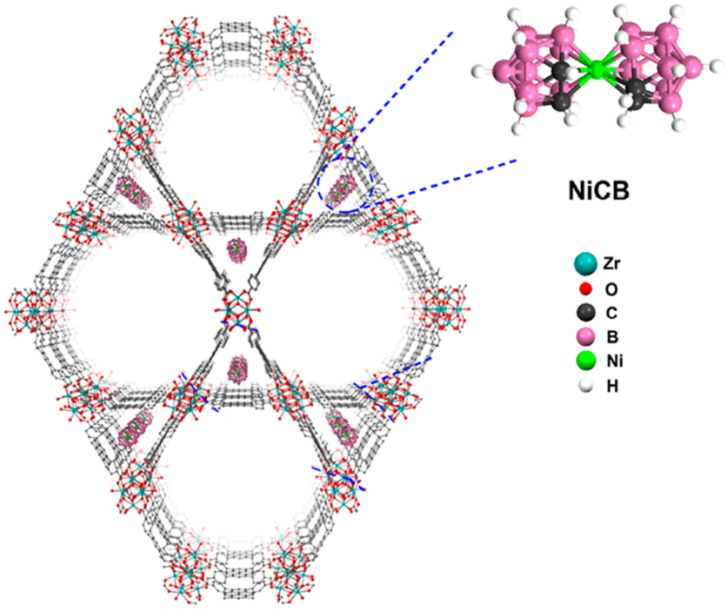

Figure 8. Crystal structure of NiCB@NU-1000 at 100K showing only one NiCB orientation for clarity. Adapted from reference 38.

2.9. Silver Metal Clusters-Induced Electrical Photoconductivity of Rb-CD-MOF

Grzybowski et al.[39] incorporated silver nanocrystals (AgNCs) into the cavities of a porous MOF called Rb-CD-MOF (Figure 9) synthesized from RbOH and γ-cyclodextrin (γ-CD). Upon treatment with 10 mM

$AgNO_3$ solutions the MOF contained 1.4 vol% of encapsulated AgNCs, as determined by ICP-AES and EDX analyses. Consequently, the surface area of the MOF decreased from 914 m^2/g to 632 m^2/g after incorporation of AgNCs, however the overall porosity of the framework was retained. Electrical measurements performed on millimeter sized crystals of Rb-CD-MOF and AgNC@Rb-CD-MOF revealed their insulating nature with conductivities of ~10^{-12} S/cm and 2×10^{-11} S/cm, respectively, at room temperature. Interestingly, under high power light (1.48 W/cm^2), the conductivity of the pristine MOF increased barely to 2×10^{-11} S/cm, but that of AgNC@Rb-CD-MOF surged 10^4 times to 2.15×10^{-7} S/cm, rendering the material photoconductive. The authors proposed that charge transport in the doped MOF took place via light-assisted tunneling between the AgNCs located within the pores. However, given the high irradiation power needed for conductivity increase, the light was not only responsible for optical excitation, but also caused thermal excitation, i.e., heating. To delineate the effects of optical and thermal activations, the conductivity of AgNC@Rb-CD-MOF was measured under constant light intensity at variable temperatures and at constant temperature under variable light intensity. In both cases, the ohmic responses were observed with small increments in conductivity (up to ~10^{-8} S/cm), suggesting that both direct optical excitation and indirect thermal excitation were responsible for the improved electrical conductivity of the doped material.

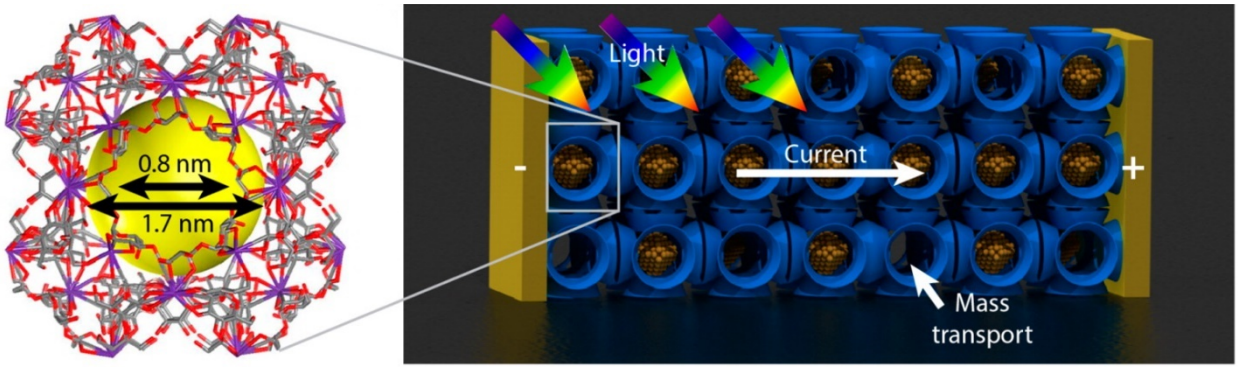

Figure 9. Left: Ru-CD-MOF crystal structure featuring cavities of 1.7 nm with channels of 0.8 nm. Right: Schematic representation of the AgNCs inside the MOF pores where not all cavities are filled. Adapted from reference 39.

2.10. PEDOT-Induced Electrical Conductivity of MIL-101(Cr) MOF

Another approach to improve the electrical conductivity of MOFs involved incorporation of conductive polymers (CP) inside its pores. Uemura et al.[40] prepared a series of MOF-CP composites in two steps, first by loading MIL-101(Cr) pores with 3,4-ethylenedioxythiophene (EDOT) monomer (up to 160±10% of the

MOF empty mass) and then performing oxidative polymerization of the encapsulated monomers by exposing the doped MOF to I_2 vapors (Figure 10), which polymerized 82–86% of EDOT into PEDOT as estimated by XRF based on the Cr/S ratio. BET analysis revealed that the surface area of MIL-101(Cr) (**1**) decreased from ~3100 m^2/g to 803 m^2/g in **1⊃PEDOT(57)** (where 57 was the mass fraction of PEDOT in the composite material). The electrochemical impedance spectroscopy performed on pressure-sintered pellets of **1** and **1⊃PEDOT(57)** revealed their respective electrical conductivities of $<10^{-11}$ and 1.1×10^{-3} S/cm, which amounted to 10^8 times improvement in the latter. The higher conductivity of MOF-PC composite was attributed to charge transport through the PEDOT network and iodine/iodide species trapped inside the MOF pores acting as dopants. Furthermore, the conductivity of **1⊃PEDOT(57)** composite was higher than those obtained for composites prepared from **1** and other conducting polymers, such as unsubstituted polythiophene and polypyrrole using a similar approach, indicating that the nature of the conductive polymer played an important role on this electronic property. In addition, another composite of La(1,3,5-benzenetrisbenzoate) featuring 1D channels and PEDOT was prepared in a similar manner resulting in a conductivity of only 2.3×10^{-8} S/cm, which was much lower than that of **1⊃PEDOT(57)**, and attributed to low connectivity between isolated polymers chain inside the 1D channels.

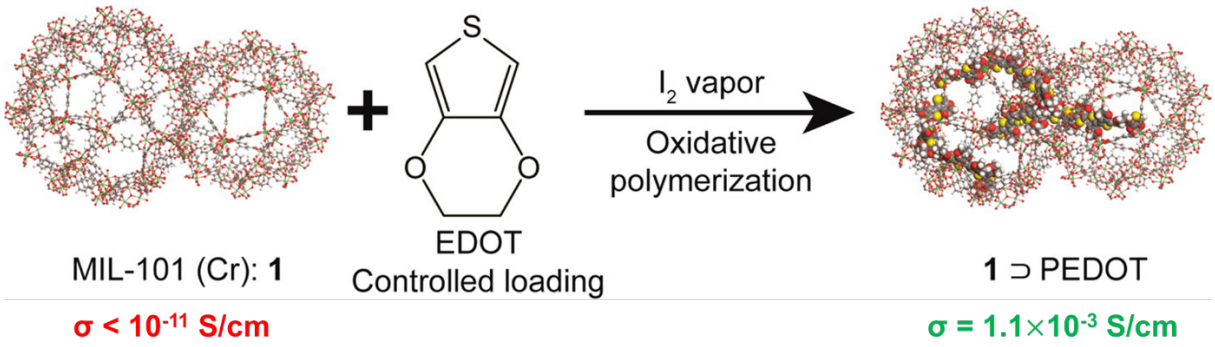

Figure 10. Schematic representation of the preparation of composite **1⊃PEDOT** and their corresponding conductivity values. Adapted from reference 40.

3. Ionic Conductivity of Doped MOFs

3.1. Li^+-Induced Electrical Conductivity of Mg_2(dobdc) MOF-74

Li^+ ion conductivity is another attractive feature of MOFs because it opens the door for using MOFs as solid electrolytes or even electrode materials in rechargeable batteries. By imbuing an activated MOF-74 analogue, Mg_2(dobdc) ($dobdc^{4-}$ = 1,4-dioxido-2,5-benzenedicarboxylate) containing Mg^{2+} sites with LiO^iPr and $LiBF_4$ salts (Figure 11), Long et al.[41] prepared Mg_2(dobdc)•0.35LiO^iPr•0.25$LiBF_4$•EC•DEC (EC =

ethylene carbonate, DEC = diethyl carbonate). The ionic conductivity of pressed pellets of this Li^+-doped MOF-74 measured by two-point *ac* impedance spectroscopy surged to 3.1×10^{-4} S/cm from 1.8×10^{-6} S/cm observed for the undoped material. The conductivity improvement relied on the availability of vacant coordination sites on Mg^{2+} nodes in activated MOF that could accommodate $^{i}PrO^{-}$ anions and ethylene carbonate molecules on these nodes, which, in turn, captured a large number of Li^+ cations and helped them to move along the channels. Variable temperature conductivity measurements of the Li^+-doped MOF-74 pellets showed a low thermal activation energy of 0.15 eV, indicating a facile ionic conduction through the grafted material. Owing to its relatively high conductivity and the low activation energy, this material could be classified as a superionic conductor, which could potentially serve as a solid lithium electrolyte in rechargeable batteries.

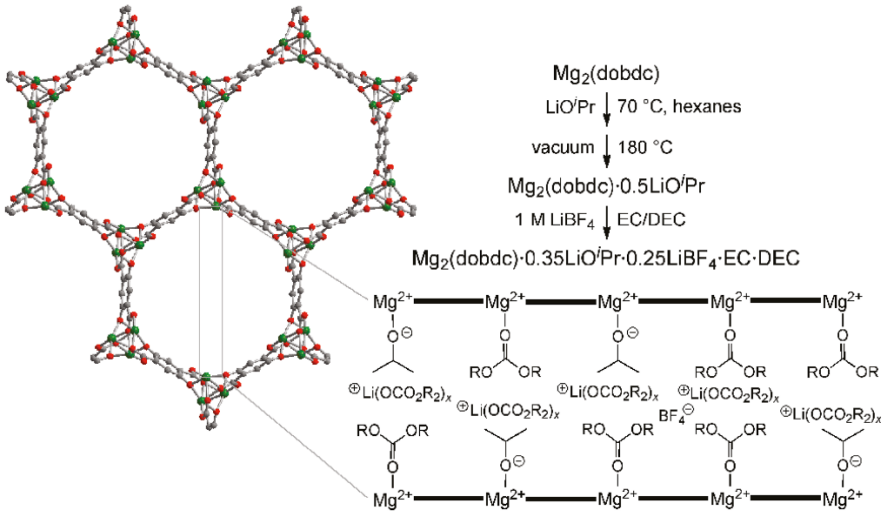

Figure 11. The structure of Mg_2(dobdc) MOF-74 showing the proposed binding of the lithium alkoxide, EC and DEC solvent molecules after the grafting process. Adapted from reference 41.

3.2. Li^+-Induced Electrical Conductivity of UiO-66 MOF

Adopting a similar approach, later on the same group designed a solid Li^+ ion electrolyte by post-synthetically modifying the nodes of UiO-66 MOF ($Zr_6O_4(OH)_4(BDC)_6$) (Figure 12).[42] Dehydration of the metal cluster under vacuum at 300 °C created coordinative-unsaturated Zr^{4+} sites, approximately 25% of which were then grafted with lithium *tert*-butoxide. The ionic conductivity of pressed pellets of free-flowing powder of this material reached 1.8 x 10^{-5} S/cm at room temperature. Apparently, this grafting process was more effective for ionic conductivity as the bulky aliphatic group of alkoxide anions shielded the negative charges and allowed the Li^+ cations to move more freely than localized negative charges achieved through

direct deprotonation. For example, the ionic conductivity of a deprotonated UiO-66 sample (rehydrated and then soaked in lithium tert-butoxide) was only 3.3×10^{-6} S/cm, almost an order of magnitude lower than the grafted UiO-66 MOF, even though the Li^+ content in the former was four times greater than the latter. Furthermore, the activation energy of the grafted material is 0.18 eV, whereas that for the deprotonated material is 0.35eV, corroborating that the interaction between Li^+ and the localized negative charge was stronger in the deprotonated material.

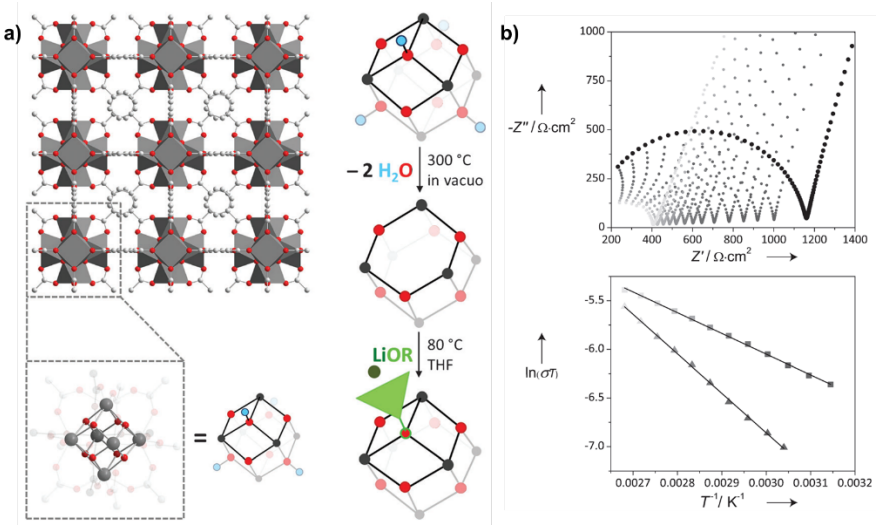

Figure 12. a) Representation of the grafting process on UiO-66 MOF and b) Top: Nyquist plots of grafted-UiO-66 MOF at various temperatures (313-383 K from dark to light grey), the data collected at 293 K is represented in black. Bottom: Arrhenius plots of grafted-UiO-66 MOF (■) and UiO-66 MOF directly deprotonated with LiO*t*Bu (▲). Adapted from reference 42.

3.3. Li^+-Induced Electrical Conductivity of Cu(I)–sulfonate MOF

Recently, we have constructed a 2D sheet-like neutral Cu(I)–sulfonate MOF using NDI ligands functionalized with two sulfonate groups (DSNDI),[43] which could simultaneously bind guest Li^+ cations with the carbonyl groups as well as uncoordinated sulfonate oxygen atoms and charge diffuse perchlorate anions through anion–π interaction with the π-acidic NDI core (Figure 13). Electrochemical impedance measurements on in-situ pressed MOF pellets revealed that pristine MOF pellets displayed negligible intrinsic electrical conductivity (4.65×10^{-12} S/cm) at room temperature due to inadequate charge carrier density and electron delocalization pathway. However, upon infiltration of $LiClO_4$, its ionic conductivity surged million times to 2.3×10^{-6} S/cm. Variable temperature conductivity measurements further demonstrated that the Li^+-doped MOF enjoyed a fairly low activation energy (0.17 eV) for charge carrier

transport. This study represented a rare example where the Li^+ ion conductivity of MOF was not artificially influenced by the presence of highly polar organic solvents such as propylene carbonate.

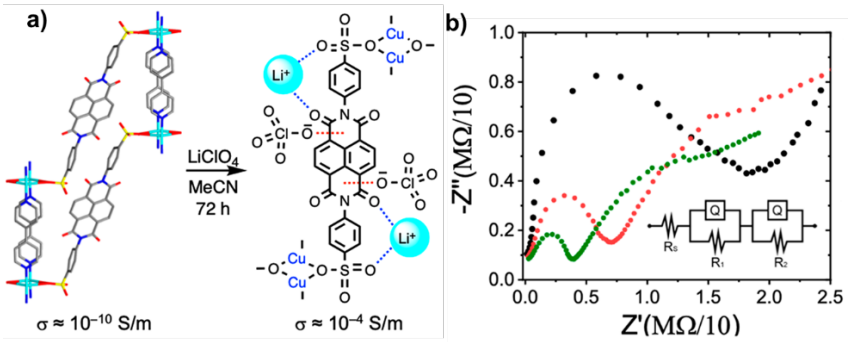

Figure 13. a) Cu(I)-sulfonate undoped MOF crystal structure and hypothetical coordination of $LiClO_4$ guest molecules after doping b) Nyquist plots of $LiClO_4$-doped Cu(I)-sulfonate MOF obtained from EIS measurements at 18°C (black), 45°C (red) and 65°C (green). Adapted from reference 43.

3.4. Li^+ and Mg^{2+}-Induced Electrical Conductivity of Cu-Azolate MOF

Dincă et al.[44] also designed a solid Li^+ and Mg^{2+} electrolyte by taking advantage of ion-pairing interactions and open anionic binding sites in a Cu-azolate MOF, $Cu_4(ttpm)_2 \cdot 0.6CuCl_2$ (H_4ttpm = tetrakis (4-tetrazollyphenyl) methane). After making the cation binding sites in parent MOF accessible through Soxhlet extraction, its ionic conductivity was tuned by introducing different salts (e.g., LiCl, LiBr, $MgCl_2$ and $MgBr_2$) with variable ion-pairing strength. However, the crystallinity of the MOF diminished significantly in the presence of LiI and it was completely destroyed by MgI_2. The pristine MOF was insulating displaying poor electrical conductivity (5.08×10^{-12} S/cm). EIS performed on different salt-soaked MOFs revealed that its Li^+ ion conductivity was inversely proportional to the ionic strength of the Li-halides—2.4×10^{-5} S/cm (MOF-LiCl), 3.2×10^{-5} S/cm (MOF-LiBr) and 1.1×10^{-4} S/cm (MOF-LiI)—which was dictated by the softness of the anion. The activation energies also followed the same trend (0.34 eV for MOF-LiCl, 0.30 eV for MOF-LiBr and 0.24 eV for MOF-LiI), however, due to weakening of Coulombic forces that immobilized the anions close to the Cu^{2+} centers with the increasing anion softness, the contribution of Li^+ ions to ionic current, i.e., the Li^+ transference number displayed an opposite trend: 0.69 for MOF-LiCl, 0.42 for MOF-LiBr and only 0.34 for MOF-LiI. The MOF also displayed a similar trend of Mg^{2+} ion conductivity and activation energy in the presence of different Mg-halide salts, with the optimum values ($\sigma = 1.3\times10^{-4}$ S/cm, E_a = 0.24 eV) in the presence of $MgBr_2$. Although these salt-soaked MOFs also contained a large amount of highly solvent polar propylene carbonate, which likely have contributed to their ionic

conductivities, this work demonstrated the potential of MOFs as solid electrolytes and their tunability with the softness of the immobilized anion.

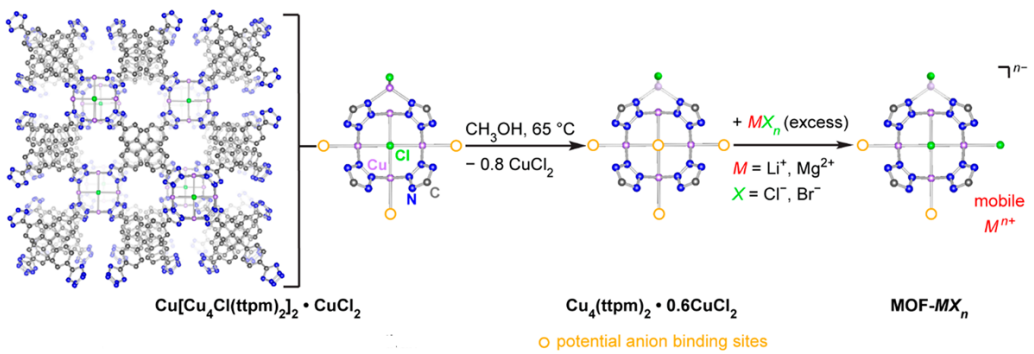

Figure 14. Synthesis of $Cu_4(ttpm)_2 \cdot 0.6CuCl_2$ and scheme of the resulting metal-halide soaked MOFs. Adapted from reference 44.

Table 1. Electrical conductivity and BET surface area of pristine and doped metal organic frameworks included in this review.

MOF doped with guest molecules	Conductivity (S/cm)	Conductivity undoped MOF (S/cm)	Surface area (m^2/g)	Surface area of undoped MOF (m^2/g)
$\{Zn_3(_{DL}\text{-lac})_2(pybz)_2]\bullet 2.5DMF\}_n/I_2$	3.42×10^{-3} σ 1.64×10^{-4}	Not reported	Not reported	762.5
$Cu[Ni(pdt)_2]/I_2$	1×10^{-4}	1×10^{-8}	Not reported	423
$Co_3(NDC)_3/I_2$	1.88×10^{-6}	Not reported	Not reported	Not reported
HKUST-1/TCNQ	7×10^{-2}	1×10^{-8}	214±0.5	1844±4
$[Zn_2(TCPB)(BPDPNDI)]/MV^{2+}$	2.3×10^{-5}	6×10^{-7}	Not reported	65
DSNDI-MOF-74/TTF	*Not reported*	Not reported	1698	2044
NU-901/C_{60}	$\sim10^{-3}$	10^{-14}	1550	2120
NU-1000/NiCB	2.7×10^{-7}	Not measurable	1260	2215
Rb-CD-MOF/AgNCs and Light	2.15×10^{-7}	2×10^{-11}	632	914
MIL-101(Cr)/PEDOT	1.1×10^{-3}	$<10^{-11}$	803	3100

Mg_2(dobdc)MOF-74/Li^+	3.1×10^{-4}	1.8×10^{-6}	Not reported	Not reported
UiO-66/Li^+	1.8×10^{-5}	Not reported	510±9	1020±3
Cu(I)-sulfonate MOF/Li^+	2.3×10^{-6}	4.65×10^{-12}	Not reported	20
Cu-azolate MOF/LiI	1.1×10^{-4}	5.08×10^{-12}	Not reported	Not reported
Cu-azolate MOF/$MgBr_2$	1.3×10^{-4}	5.08×10^{-12}	Not reported	Not reported

4. Conclusions and Outlook

The representative examples discussed above demonstrated that the electrical and ionic conductivities of porous MOFs could be easily improved by introducing complementary redox-active guests that imbue them with mobile charge carriers and create new charge movement pathways that were not originally present in pristine MOFs. This strategy is broadly adoptable and turns one of the downsides of porous frameworks, i.e., poor charge diffusion capability, into a strength by filling the voids with complementary guests that can participate in electronic interactions with the MOF ligands and nodes. In addition to improving MOF's electrical and ionic conductivities, which opened the door for using MOFs in molecular electronics, photovoltaics, and energy storage devices, partial preservation of MOF's porosity even after guest encapsulation can pave the way for electrocatalysis, chemiresistive sensing, and other sophisticated applications.

Acknowledgement

The authors acknowledge the financial support from the National Science Foundation (Award DMR-1809092).

References:

(1) Furukawa, H.; Cordova, K. E.; O'Keeffe, M.; Yaghi, O. M. The Chemistry and Applications of Metal-Organic Frameworks. *Science* **2013**, *341*, 974–986.

(2) Li, B.; Chrzanowski, M.; Zhang, Y.; Ma, S. Applications of Metal-Organic Frameworks Featuring Multi-Functional Sites. *Coord. Chem. Rev.* **2016**, *307*, 106–129.

(3) Yuan, S.; Feng, L.; Wang, K.; Pang, J.; Bosch, M.; Lollar, C.; Sun, Y.; Qin, J.; Yang, X.; Zhang, P.; Wang, Q.; Zou, L.; Zhang, Y.; Zhang, L.; Fang, Y.; Li, J.; Zhou, H.-C. Stable Metal-Organic Frameworks: Design, Synthesis, and Applications. *Adv. Mater.* **2018**, *30*, 1704303 (1-35).

(4) Sumida, K.; Rogow, D. L.; Mason, J. A.; McDonald, T. M.; Bloch, E. D.; Herm, Z. R.; Bae, T.; Long, J. R. Carbon Dioxide Capture in Metal–Organic Frameworks. *Chem. Rev.* **2012**, *112*, 724–781.

(5) Horcajada, P.; Gref, R.; Baati, T.; Allan, P. K.; Maurin, G.; Couvreur, P.; Férey, G.; Morris, R. E.; Serre, C. Metal–Organic Frameworks in Biomedicine. *Chem. Rev.* **2012**, *112*, 1232–1268.

(6) Liu, J.; Chen, L.; Cui, H.; Zhang, J.; Zhang, L.; Su, C.-Y. Applications of Metal–Organic Frameworks in Heterogeneous Supramolecular Catalysis. *Chem. Soc. Rev.* **2014**, *43*, 6011–6061.

(7) Dolgopolova, E. A.; Shustova, N. B. Metal–Organic Framework Photophysics: Optoelectronic Devices, Photoswitches, Sensors, and Photocatalysts. *MRS Bull.* **2016**, *41*, 890–896.

(8) Lustig, W. P.; Mukherjee, S.; Rudd, N. D.; Desai, A. V.; Li, J.; Ghosh, S. K. Metal–Organic Frameworks: Functional Luminescent and Photonic Materials for Sensing Applications. *Chem. Soc. Rev.* **2017**, *46*, 3242–3285.

(9) Stavila, V.; Talin, A. A.; Allendorf, M. D. MOF-Based Electronic and Opto-Electronic Devices. *Chem. Soc. Rev.* **2014**, *43*, 5994–6010.

(10) D'Alessandro, D. M. Exploiting Redox Activity in Metal–Organic Frameworks: Concepts, Trends and Perspectives. *Chem. Commun.* **2016**, *52*, 8957–8971.

(11) Allendorf, M. D.; Schwartzberg, A.; Stavila, V.; Talin, A. A. A Roadmap to Implementing Metal-Organic Frameworks in Electronic Devices: Challenges and Critical Directions. *Chem. Eur. J.* **2011**, *17*, 11372–11388.

(12) Hendon, C. H.; Tiana, D.; Walsh, A. Conductive Metal–Organic Frameworks and Networks: Fact or Fantasy? *Phys. Chem. Chem. Phys.* **2012**, *14*, 13120.

(13) Sun, L.; Campbell, M. G.; Dincă, M. Electrically Conductive Porous Metal-Organic Frameworks. *Angew. Chem. Int. Ed.* **2016**, *55*, 3566–3579.

(14) Leong, C. F.; Usov, P. M.; D'Alessandro, D. M. Intrinsically Conducting Metal–Organic Frameworks. *MRS Bull.* **2016**, *41*, 858–864.

(15) Hmadeh, M.; Lu, Z.; Liu, Z.; Gándara, F.; Furukawa, H.; Wan, S.; Augustyn, V.; Chang, R.; Liao, L.; Zhou, F.; Perre, E.; Ozolins, V.; Suenaga, K.; Duan, X.; Dunn, B.; Yamamto, Y.; Terasaki, O.; Yaghi, O. M. New Porous Crystals of Extended Metal-Catecholates. *Chem. Mater.* **2012**, *24*, 3511–3513.

(16) Sheberla, D.; Sun, L.; Blood-Forsythe, M. A.; Er, S.; Wade, C. R.; Brozek, C. K.; Aspuru-Guzik, A.; Dincă, M. High Electrical Conductivity in Ni_3(2,3,6,7,10,11-Hexaiminotriphenylene)$_2$, a Semiconducting Metal–Organic Graphene Analogue. *J. Am. Chem. Soc.* **2014**, *136*, 8859–8862.

(17) Campbell, M. G.; Sheberla, D.; Liu, S. F.; Swager, T. M.; Dincă, M. Cu 3 (Hexaiminotriphenylene) 2 : An Electrically Conductive 2D Metal-Organic Framework for Chemiresistive Sensing. *Angew. Chem. Int. Ed.* **2015**, *54*, 4349–4352.

(18) Kambe, T.; Sakamoto, R.; Kusamoto, T.; Pal, T.; Fukui, N.; Hoshiko, K.; Shimojima, T.; Wang, Z.; Hirahara, T.; Ishizaka, K.; Hasegawa, S.; Liu, F.; Nishihara, H. Redox Control and High Conductivity of Nickel Bis(Dithiolene) Complex π-Nanosheet: A Potential Organic Two-Dimensional Topological Insulator. *J. Am. Chem. Soc.* **2014**, *136*, 14357–14360.

(19) Huang, X.; Sheng, P.; Tu, Z.; Zhang, F.; Wang, J.; Geng, H.; Zou, Y.; Di, C.; Yi, Y.; Sun, Y.; Xu, W.; Zhu, D. A Two-Dimensional π–d Conjugated Coordination Polymer with Extremely High Electrical Conductivity and Ambipolar Transport Behaviour. *Nat. Commun.* **2015**, *6*, 7408.

(20) Pal, T.; Kambe, T.; Kusamoto, T.; Foo, M. L.; Matsuoka, R.; Sakamoto, R.; Nishihara, H. Interfacial Synthesis of Electrically Conducting Palladium Bis(Dithiolene) Complex Nanosheet. *Chempluschem* **2015**, *80*, 1255–1258.

(21) Wu, G.; Huang, J.; Zang, Y.; He, J.; Xu, G. Porous Field-Effect Transistors Based on a Semiconductive Metal-Organic Framework. *J. Am. Chem. Soc.* **2017**, *139*, 1360–1363.

(22) Yao, M. S.; Lv, X. J.; Fu, Z. H.; Li, W. H.; Deng, W. H.; Wu, G. D.; Xu, G. Layer-by-Layer Assembled Conductive Metal–Organic Framework Nanofilms for Room-Temperature Chemiresistive Sensing. *Angew. Chemie - Int. Ed.* **2017**, *56*, 16510–16514.

(23) Li, W.-H.; Ding, K.; Tian, H.-R.; Yao, M.-S.; Nath, B.; Deng, W.-H.; Wang, Y.; Xu, G. Conductive Metal-Organic Framework Nanowire Array Electrodes for High-Performance Solid-State Supercapacitors. *Adv. Funct. Mater.* **2017**, *27*, 1702067.

(24) Yao, M.-S.; Xiu, J.-W.; Huang, Q.-Q.; Li, W.-H.; Wu, W.-W.; Wu, A.-Q.; Cao, L.-A.; Deng, W.-H.; Wang, G.-E.; Xu, G. Van Der Waals Heterostructured MOF-on-MOF Thin Films: Cascading Functionality to Realize Advanced Chemiresistive Sensing. *Angew. Chem. Int. Ed.* **2019**, *58*, 14915–14919.

(25) Campbell, M. G.; Liu, S. F.; Swager, T. M.; Dincə, M. Chemiresistive Sensor Arrays from Conductive 2D Metal-Organic Frameworks. *J. Am. Chem. Soc.* **2015**, *137*, 13780–13783.

(26) Takaishi, S.; Hosoda, M.; Kajiwara, T.; Miyasaka, H.; Yamashita, M.; Nakanishi, Y.; Kitagawa, Y.; Yamaguchi, K.; Kobayashi, A.; Kitagawa, H. Electroconductive Porous Coordination Polymer $Cu[Cu(Pdt)_2]$ Composed of Donor and Acceptor Building Units. *Inorg. Chem.* **2009**, *48*, 9048–9050.

(27) Gándara, F.; Uribe-Romo, F. J.; Britt, D. K.; Furukawa, H.; Lei, L.; Cheng, R.; Duan, X.; O'Keeffe, M.; Yaghi, O. M. Porous, Conductive Metal-Triazolates and Their Structural Elucidation by the Charge-Flipping Method. *Chem. Eur. J.* **2012**, *18*, 10595–10601.

(28) Darago, L. E.; Aubrey, M. L.; Yu, C. J.; Gonzalez, M. I.; Long, J. R. Electronic Conductivity, Ferrimagnetic Ordering, and Reductive Insertion Mediated by Organic Mixed-Valence in a Ferric Semiquinoid Metal–Organic Framework. *J. Am. Chem. Soc.* **2015**, *137*, 15703–15711.

(29) Sun, L.; Hendon, C. H.; Minier, M. A.; Walsh, A.; Dincă, M. Million-Fold Electrical Conductivity Enhancement in Fe 2 (DEBDC) versus Mn 2 (DEBDC) (E = S, O). *J. Am. Chem. Soc.* **2015**, *137*, 6164–6167.

(30) Allendorf, M. D.; Foster, M. E.; Léonard, F.; Stavila, V.; Feng, P. L.; Doty, F. P.; Leong, K.; Ma, E. Y.; Johnston, S. R.; Talin, A. A. Guest-Induced Emergent Properties in Metal-Organic Frameworks. *J. Phys. Chem. Lett.* **2015**, *6*, 1182–1195.

(31) Zeng, M. H.; Wang, Q. X.; Tan, Y. X.; Hu, S.; Zhao, H. X.; Long, L. S.; Kurmoo, M. Rigid Pillars and Double Walls in a Porous Metal-Organic Framework: Single-Crystal to Single-Crystal, Controlled Uptake and Release of Iodine and Electrical Conductivity. *J. Am. Chem. Soc.* **2010**, *132*, 2561–2563.

(32) Kobayashi, Y.; Jacobs, B.; Allendorf, M. D.; Long, J. R. Conductivity, Doping, and Redox Chemistry of a Microporous Dithiolene-Based Metal-Organic Framework. *Chem. Mater.* **2010**, *22*, 4120–4122.

(33) Lee, D. Y.; Kim, E. K.; Shrestha, N. K.; Boukhvalov, D. W.; Lee, J. K.; Han, S. H. Charge Transfer-Induced Molecular Hole Doping into Thin Film of Metal-Organic Frameworks. *ACS Appl. Mater. Interfaces* **2015**, *7*, 18501–18507.

(34) Talin, A. A.; Centrone, A.; Ford, A. C.; Foster, M. E.; Stavila, V.; Haney, P.; Kinney, R. A.; Szalai, V.; El Gabaly, F.; Yoon, H. P.; Léonard, F.; Allendorf, M. D. Tunable Electrical Conductivity in Metal-Organic Framework Thin-Film Devices. *Science* **2014**, *343*, 66–69.

(35) Guo, Z.; Panda, D. K.; Maity, K.; Lindsey, D.; Parker, T. G.; Albrecht-Schmitt, T. E.; Barreda-

Esparza, J. L.; Xiong, P.; Zhou, W.; Saha, S. Modulating the Electrical Conductivity of Metal-Organic Framework Films with Intercalated Guest π-Systems. *J. Mater. Chem. C* **2016**, *4*, 894–899.

(36) Guo, Z.; Panda, D. K.; Gordillo, M. A.; Khatun, A.; Wu, H.; Zhou, W.; Saha, S. Lowering Band Gap of an Electroactive Metal-Organic Framework via Complementary Guest Intercalation. *ACS Appl. Mater. Interfaces* **2017**, *9*, 32413–32417.

(37) Goswami, S.; Ray, D.; Otake, K. I.; Kung, C. W.; Garibay, S. J.; Islamoglu, T.; Atilgan, A.; Cui, Y.; Cramer, C. J.; Farha, O. K.; Hupp, J. T. A Porous, Electrically Conductive Hexa-Zirconium(Iv) Metal-Organic Framework. *Chem. Sci.* **2018**, *9*, 4477–4482.

(38) Kung, C. W.; Otake, K.; Buru, C. T.; Goswami, S.; Cui, Y.; Hupp, J. T.; Spokoyny, A. M.; Farha, O. K. Increased Electrical Conductivity in a Mesoporous Metal-Organic Framework Featuring Metallacarboranes Guests. *J. Am. Chem. Soc.* **2018**, *140*, 3871–3875.

(39) Han, S.; Warren, S. C.; Yoon, S. M.; Malliakas, C. D.; Hou, X.; Wei, Y.; Kanatzidis, M. G.; Grzybowski, B. A. Tunneling Electrical Connection to the Interior of Metal–Organic Frameworks. *J. Am. Chem. Soc.* **2015**, *137*, 8169–8175.

(40) Le Ouay, B.; Boudot, M.; Kitao, T.; Yanagida, T.; Kitagawa, S.; Uemura, T. Nanostructuration of PEDOT in Porous Coordination Polymers for Tunable Porosity and Conductivity. *J. Am. Chem. Soc.* **2016**, *138*, 10088–10091.

(41) Wiers, B. M.; Foo, M. L.; Balsara, N. P.; Long, J. R. A Solid Lithium Electrolyte via Addition of Lithium Isopropoxide to a Metal-Organic Framework with Open Metal Sites. *J. Am. Chem. Soc.* **2011**, *133*, 14522–14525.

(42) Ameloot, R.; Aubrey, M.; Wiers, B. M.; Gõmora-Figueroa, A. P.; Patel, S. N.; Balsara, N. P.; Long, J. R. Ionic Conductivity in the Metal-Organic Framework UiO-66 by Dehydration and Insertion of Lithium Tert-Butoxide. *Chem. Eur. J.* **2013**, *19*, 5533–5536.

(43) Panda, D. K.; Maity, K.; Palukoshka, A.; Ibrahim, F.; Saha, S. Li^{+} Ion-Conducting Sulfonate-Based Neutral Metal–Organic Framework. *ACS Sustain. Chem. Eng.* **2019**, *7*, 4619–4624.

(44) Miner, E. M.; Park, S. S.; Dincă, M. High Li^{+} and Mg^{2+} Conductivity in a Cu-Azolate Metal-Organic Framework. *J. Am. Chem. Soc.* **2019**, *141*, 4422–4427.